Loss of the protein disrupted in schizophrenia 1 (DISC1) impairs cardiac resistance against ischemia.

Running title: The protein DISC1 a novel player in ischemic heart disease?

Gurdeep Marwarha[1], Maria J. Pinho[1], Nathan R Scrimgeour[1], Katrine Hordnes Slagsvold[1,2], Alexander Wahba[1,2], Ragnhild E Røsbjørgen[1, 2], Francisco J. Enguita[3], Kun Yang[4], Koko Ishizuka[4], Carlos Andrés Acosta Casas[4], Kristine Pettersen[5,6], Geir Bjørkøy[5,6], Akira Sawa[4], Morten A Høydal[1]*

[1] Norwegian University of Science and Technology (NTNU), Faculty of Medicine and Health, Trondheim, Norway. Department of Circulation and Medical Imaging, Trondheim, Norway.
[2] Dept. of thoracic surgery and dept. of Cardiology; St. Olavs University Hospital, Trondheim, Norway.
[3] Instituto de Medicina Molecular, Faculty of Medicine, University of Lisbon, 1649-028 Lisbon, Portugal.
[4] Johns Hopkins University School of Medicine, Baltimore, MD.
[5] Norwegian University of Science and Technology (NTNU). Department of Biomedical Laboratory Science, Faculty of Natural Sciences, NTNU, Trondheim, Norway.
[6] Norwegian University of Science and Technology (NTNU), Faculty of Medicine and Health, Centre of Molecular Inflammation Research, Department of Clinical and Molecular Medicine, Trondheim, Norway.

* Correspondence and requests for materials should be addressed to:

Dr. Morten Andre Høydal

Professor in Medicine

Norwegian University of Science and Technology (NTNU), Faculty of Medicine and Health,

Department of Circulation and Medical Imaging,

PO Box 8905, NO-7491 Trondheim, Norway.

e-mail: morten.hoydal@ntnu.no/ telephone: +4748134843

Supplementary Information is available for this paper.

Abstract

Treatable targets that hinder heart failure development following myocardial infarction remain limited. Through an unbiased transcriptional regulation study for ischemic heart disease, we identified the protein disrupted in schizophrenia 1 (DISC1), which has been almost solely characterized in the brain. Here, we show that loss of DISC1 is a major driver of heart disease and ischemic damage. Silencing of DISC1 sensitizes human cardiomyocyte cell lines to hypoxia, whereas DISC1 overexpression is cardioprotective. Mechanistically, we provide evidence that reduced DISC1 protein levels interrupt multiple signaling processes vital for cardiomyocyte survival whereas overexpression of DISC1 enhances pro survival signalling. The present study has implications for understanding scenarios where cardiomyocytes are unable to increase the levels of DISC1 during ischemia, e.g., in individuals with DISC1 genetic defects. Indeed, patients with severe mental illness display 20 years earlier mortality, with IHD as the greatest cause of death. The present study can thus shed light on this long-term enigma in epidemiology. Furthermore, the promising data showing activation of pro survival signalling processes with DISC1 overexpression opens new directions towards potential treatment strategies of patients suffering from ischemic heart disease.

Introduction

Ischemic heart disease (IHD) is the leading cause of death globally (Organization, 2014). Despite substantial improvements in clinical outcome, a significant share of patients still suffers from premature death after myocardial infarction (MI) (Hausenloy et al., 2017). To address this challenge, we established a new model using human inducible pluripotent stem cell-derived cardiomyocytes (hIPS-CMs) and subjected these cells to pathological hypoxic stress. Exploring the global transcriptional landscape through next-generation RNA sequencing allowed identification of key transcripts involved in the CM response to hypoxia. To our surprise, disrupted schizophrenia 1 (DISC1) was the most strikingly responsive gene in cardiomyocytes exposed to hypoxic conditions.

DISC1 was originally identified from a gene directly disrupted by a balanced chromosomal translocation t(1;11) (q42;q14.3) in a large Scottish family with a high load of major psychiatric illness (Millar et al., 2000). Today, DISC1 is viewed as an important regulator of neurodevelopment, and its loss of function can be a driver of severe mental illness, such as major depressive disorder and schizophrenia (SZ)(Brandon and Sawa, 2011; Niwa et al., 2016; Yerabham et al., 2013). At the cellular level, DISC1 is a scaffolding protein that binds to and regulates a range of signaling cascades and protein networks in neuronal cells (Brandon and Sawa, 2011; Yerabham et al., 2013). In the heart, however, no data exist on the role of DISC1, beyond which DISC1 expression is as high as in neural tissue (Ozeki et al., 2003). Interestingly, epidemiological data from patients with severe mental illness, in particular SZ, show a 20-year lower life expectancy than the general population, with IHD as the leading cause of death (Nielsen et al., 2015). Furthermore, recent reports display deteriorated cardiac function measured by echocardiography (Korkmaz et al., 2016) and MRI (Pillinger et al., 2019) in SZ patients. Myocardial T1 mapping (proton spin-lattice relaxation time), which enables detection of myocardial edema, infarction, ischemia, cardiomyopathies and diffuse fibrosis (Liu et al., 2017), further suggests that an early diffuse fibroinflammatory myocardial process in SZ patients is independent of established CVD-risk factors and could contribute to excess cardiovascular mortality (Pillinger et al., 2019). Although we cannot completely exclude the secondary influence of medication, severe mental illness comorbidities frequently include cardiovascular deficits (Pillinger et al., 2019; Sun et al., 2019).

Therefore, we hypothesized that DISC1 is not only important for the development of SZ but that loss of function or depletion of DISC1 directly renders the heart and cardiac cells more vulnerable to and prone to IHD damage. Furthermore, we hypothesize that DISC1 is a new and hitherto unknown

multifunctional protein, a potential master regulator, that orchestrates intracellular processes in the heart that are vital to resist cardiac damage caused by ischemic stress, such as myocardial infarction.

Results

Discovery of the cardiac role of DISC1 by transcriptomics

A major limitation in establishing novel treatment strategies is that most experimental studies target only single intracellular signalling pathways. The lack of success in such strategies calls for novel targets directed at multiple signalling pathways, which remains a gap in existing knowledge (Hausenloy et al., 2017). To answer this challenge, we established a new model using human inducible pluripotent stem cell-derived cardiomyocytes (hIPS-CMs) with pathological hypoxic stress stimulation. Exploring the global transcriptional landscape through next-generation RNA sequencing allowed identification of key transcripts involved in the CM response to hypoxia. Our first indication of a role for DISC1 in CMs was revealed by RNA-seq of hIPS-CMs exposed to pathological hypoxic stress for 48 hours. In hIPS-CMs, we detected 1232 significantly regulated transcripts (cut-off value adjusted $P < 0.05$) between hypoxia and normoxia. Here, we found that DISC1 scored among the most regulated coding transcripts, displaying downregulation by $Log_2FC = -2,67$ because of hypoxia (P-value = 3,41E-51) (Fig. 1A-B and Fig S1). To further explore the global transcriptional response to hypoxia in CMs, we expanded our bioinformatics analyses by generating regulatory networks that depicted negative correlations between overexpressed microRNAs (miRs) and their putative downregulated mRNA targets from our RNA-seq data. In our analyses, we found a total of 774 mir-mRNA pairs, and of these, DISC1 stood out in these analyses, targeted by as many as 26 specific miRs (Fig. 1C).

Genome-wide association study associated DISC1 with heart disease

Given the unknown role of DISC1 in the heart, we were enthusiastic to discover that several signalling pathways and interacting protein partners of DISC1 identified in a neuronal setting are similar to earlier reported candidates for cardioprotection following myocardial ischemia (Hashimoto et al.,

2006; Hausenloy et al., 2017; Ming and Song, 2009; Sciarretta et al., 2018; Zheng et al., 2012). To determine the association between DISC1 and cardiac disease, we therefore performed GWAS enrichment analysis and found a significant overrepresentation of risk genes for heart diseases among DISC1 protein interactors (P-value = 2.8E-17) (Data S1, Table S1). With these associations, we hypothesized that DISC1 is not only important for neurodevelopment and mental disorders but that loss of function or depletion of DISC1 directly renders the heart and CMs more vulnerable and prone to ischemic damage.

DISC1 expression is altered in ischemic hearts and in CMs under hypoxic stress

To determine the presence of DISC1 in cardiac cells, as well as the regulation of DISC1 in pathological conditions of IHD, we first measured mRNA expression in a rat model of myocardial infarction. Compared to sham-operated rat hearts, DISC1 was significantly upregulated in viable myocardium remote from the infarct area, whereas in the ischemic border zone region, we found unaltered expression of DISC1 transcript (Fig. 2A). Analyses in human cardiac left ventricle biopsies from post-MI HF coronary artery bypass grafting (CABG) patients displayed a tendency of increased DISC1 expression in the remote viable myocardium (Fig. 2B), indicating increased DISC1 in response to cardiac ischemia. Previous studies from neural cells have reported that the expression of DISC1 is significantly downregulated following hypoxia (Barodia et al., 2015). These data are in line with our initial discovery of the regulation of DISC1 in cardiac cells, where we found that DISC1 was significantly reduced in hIPS-CMs stimulated by long-term exposure to hypoxia (48 hours, 1% O_2) (Fig 1 A-B). Given this contradiction in DISC1 expression compared to less ischemic impacted areas of the heart, we tested shorter timepoints of hypoxia-stimulated CMs in culture. Indeed, 6 hours of hypoxia in hIPS-CMs induced significantly increased DISC1 (Fig. 2C). The hypoxic response of DISC1 expression was further tested in human AC16 CMs, which confirmed a time-dependent response, increasing up to 18 hours and thereafter declining to levels below the normoxic baseline at 48 hours and 60 hours (Fig. 2D-E, Isoform specificity presented in Fig S2). Our data indicate that upregulation of DISC1 could be

an important component for increasing resistance against hypoxic stress. We therefore hypothesized that loss of functional ability to augment DISC1 during ischemic and/or hypoxic stress causes further ischemic damage to the heart and CMs.

Loss of DISC1 increases myocardial infarction size

To test whether loss of DISC1 causes greater ischemic damage, we used a mouse model with a DISC1-locus deletion (DISC1-locus impairment (DISC1-LI), as previously described.(Niwa et al., 2016) We found that loss of DISC1 caused significantly larger infarct size following ischemia-reperfusion in a Langendorff coronary perfusion infract model. Thirty minutes of global ischemia followed by 2 hours of reperfusion in isolated DISC1-Li mouse hearts vs. WT. DISC1-Li mice displayed larger infarct sizes in both male (130% larger) and female mice (73% larger) (Fig. 3 A-C). These data strengthen the hypothesis that loss of DISC1 exacerbates ischemic damage.

Loss of DISC1 exacerbates CM vulnerability to hypoxic stress whereas overexpression facilitate survival

Lack of oxygen and essential nutrients causes metabolic acidosis, Ca^{2+} overload and accumulation of ROS (Ertracht et al., 2014; Halestrap et al., 2007). Mitochondrial Ca^{2+} overload triggers mitochondrial depolarization, swelling and opening of the mitochondrial permeability transition pore (mPTP) (Griffiths and Halestrap, 1995; Ruiz-Meana et al., 2009), eventually causing cell death (Hausenloy and Yellon, 2003). To determine the consequence of altered DISC1 expression on CM death and viability, we tested both DISC1 silencing by shRNA-DISC1 or overexpression using a plasmid DISC1 expression vector in several lines of functional assays. Silencing of DISC1 significantly sensitized cells to hypoxic stress and increased cell death (Fig. 3D), reduced cell viability and reduced proliferation (Fig S3). Conversely, DISC1 overexpression displayed a profound protective effect against cell death (Fig. 3E). Cell viability and cell proliferation were also significantly increased by overexpression of DISC1 (Fig S3). Opening of the mPTP and translocation and formation of BAX pores at the mitochondrial membrane commonly cause (CytC) release from the mitochondria to the cytosol (Zhang et al., 2017). In turn, the

release of CytC activates downstream apoptotic cascades, such as caspase-3. Indeed, release of CytC from mitochondria to the cytosol was observed following hypoxia in AC16 CMs; shRNA-DISC1 exacerbated the release of CytC from the mitochondria to the cytosol during hypoxia (Fig. 3F), whereas in contrast, CytC release was reduced following DISC1 overexpression (Fig. 3G), facilitating cell survival. Consistently, caspase-3 activation by hypoxia was exacerbated by DISC1 depletion (Fig. 3H), whereas ectopically expressed DISC1 mitigated the activity of caspase-3 (Fig. 3I). One explanation for the increased cell death induced by DISC1 knockdown could be the direct protein-protein interaction between DISC1 and GSK3β, which was previously reported in neural cells(Ming and Song, 2009). To determine if this is the case in CMs, we first verified the direct interaction between DISC1-GSK3β by Co-IP (Fig S4). Furthermore, we confirmed that DISC1 silencing indeed increased GSK3β activity (Fig. 3J), whereas DISC1 overexpression reduced GSK3β activity (Fig. 3K). Changes in GSK3β activity were supported by altered phosphorylation of its $pSer^{9}$ inhibitory site (Fig S4). These data confirm an important role of DISC1 in suppressing GSK3β activity, leading to enhanced CM resistance against hypoxia-induced apoptosis(Ohori et al., 2008) (Fig. 3L), thus rationalizing the hypothesis that DISC1 orchestrates intracellular processes to maintain resistance against ischemic damage and hypoxic stress.

Reduced DISC1 deteriorates cardioprotective reperfusion injury salvage kinase (RISK), mTOR and CREB

The cardioprotective effects of the RISK pathway are largely driven by the pro-survival kinase Akt, a downstream target phosphorylated by phosphoinositide 3-kinase (PI3K) signalling.(Fayard et al., 2005),(Cross et al., 2000) $pThr^{308}$Akt was reduced following hypoxia. DISC1 silencing precipitated a further reduction in $pThr^{308}$Akt, whereas increased DISC1 expression, in contrast, tended to increase $pThr^{308}$ Akt (Fig. 4A-B). $pSer^{473}$Akt was also significantly reduced by hypoxia and even further decreased by shRNA-DISC1. In contrast, increased expression of DISC1 caused a significant increase in $pSer^{473}$Akt (Fig 4C-D). Several studies show the potential for increased phosphorylation of Akt in mediating cardioprotection after ischemia via inhibition of the Bcl-2-associated death promoter (BAD) (Kunuthur

et al., 2012; Li et al., 2011; Matsui et al., 2001), Bcl-2-associated X protein (BAX)(Datta et al., 1997) and glycogen synthase kinase-3ß (GSK3β) (Juhaszova et al., 2004). Our data indicate, thus, that DISC1 is an important positive modulator of the cardioprotective RISK pathway.

Furthermore, pSer^{473} Akt is regulated upstream by the mechanistic target of rapamycin (mTOR)2, whose activity is enhanced by pSer^{2481}, and previous studies have shown that mTOR activation is necessary for full activation of Akt and cardioprotection (Yano et al., 2014). To confirm the effect of DISC1 modulation on mTOR, we custom designed an mTOR1/2 activity assay that distinguished between the two complexes. Hypoxia reduced the activity of both complexes; DISC1 silencing reduced both mTORC1 and mTORC2 activity both in normoxia and under hypoxic conditions (Fig. 4E-F), whereas DISC1 overexpression caused significantly increased activity (Fig. 4G-H). The phosphorylation status of both pSer^{2481} and pSer^{2448}mTOR supports this observation (Fig S5 A-D). These data support the idea that loss of DISC1 removes the acute cardioprotective effect of mTORC2 and Akt, whereas higher levels of DISC1 enhance these signalling cascades and thus provide resistance against cardiac damage.

Furthermore, Akt activates cAMP response element-binding protein (CREB) by phosphorylation (pSer^{133}CREB), which is known to enhance cardioprotection against ischemia in the heart,(Marais et al., 2008) and in neural cells against cerebral ischemia reperfusion injury.(Teng et al., 2019) pSer^{133}CREB was significantly reduced by hypoxia; shRNA-DISC1 reduced the low pSer^{133}CREB levels further, whereas pSer^{133}CREB was significantly increased by overexpression of DISC1 (Fig. 4I-J). The changes observed with CREB under hypoxia and modulation by DISC1 expression align nicely with the changes observed in Akt. However, CREB is also phosphorylated by PKA at pSer^{133}. Given that DISC1 directly interacts with and reduces the activity of PDE4(Soares et al., 2011), which would in theory augment PKA activity, we tested the downstream effects by measuring the catalytic C subunit of cyclic AMP-dependent protein kinase A (PKA), which requires phosphorylation at Thr^{197} for full activity. Indeed, hypoxia led to significantly reduced pThr^{197}PKA; DISC1 silencing caused a further

reduction in pThr^{197}PKA, whereas DISC1 overexpression restored the pThr^{197}PKA to levels comparable to normoxic EV control (Fig. S6). Taken together, DISC1 may thus activate CREB via both Akt and PKA.

Reduced DISC1 inactivates STAT3 signaling via ERK1/2 and mTOR

A second arm of the ischemic cardioprotective pathways is the survivor activating factor enhancement (SAFE) pathways, which refer to the classical canonical activation of Janus kinase (JAK)/signal transducer and activator of transcription 3 (STAT3) and pTyr^{705} STAT3. pTyr^{705} STAT3 causes translocation into the nucleus and activates transcription of carriers of cardioprotection.(Pipicz et al., 2018) Neuregulin-1 (NRG-1) is one of the activators of JAK/STAT3, and data from neuronal cells show that DISC1 is an important component in regulating this signalling (Unda et al., 2016). NRG-1 activation reduced apoptosis after hypoxia-reoxygenation and reduced MI size following ischemia/reperfusion (Fang et al., 2017) Therefore, we first tested the activation of canonical JAK/STAT3 activation by measuring pTyr^{705} STAT3. In our data, however, we did not find alterations in pTyr^{705} STAT3 in response to hypoxia or by shRNA-DISC1 or DISC1 overexpression (Fig S7). However, STAT3 can also be activated indirectly via the mTOR and ERK1/2 pathways by phosphorylation at pSer^{727} STAT3 (Pipicz et al., 2018; Yokogami et al., 2000). Previous data in a neuronal setting have shown that loss of DISC1 suppresses Erk1/2 signalling (Hashimoto et al., 2006; Zheng et al., 2012). Therefore, we tested the effect of DISC1 modulation of ERK1/2. Indeed, under normoxia, DISC1 knockdown caused significantly reduced ERK1/2 activity. Hypoxia increased pERK1/2, whereas under these conditions, shRNA did not alter the expression (Fig. 5A). DISC1 overexpression, however, induced a significant increase in pERK1/2 under hypoxic conditions (Fig. 5B). Given that both ERK1/2 and mTOR (as presented above) are modulated by DISC1, we quantified pSer^{727}STAT3. Indeed, hypoxia induced a significant reduction in pSer^{727} STAT3. DISC1 knockdown further reduced the already low expression (NS), whereas DISC1 overexpression caused a significant increase in pSer^{727} STAT3 (Fig. 5C-D).

pSer^{727} STAT3 leads to its translocation to both the nucleus and to mitochondria (Fig. 5E). In the mitochondria, p^{Ser727}STAT3 influences mitochondrial ATP production, inhibits the opening of the mPTP,

reduces the production of reactive oxygen species and thus enhances cardioprotection.(Pipicz et al., 2018) To determine the potential translocation of STAT3 from mitochondria caused by lower pSer^{727} during hypoxia and by DISC1 knockdown, we first confirmed that hypoxia reduced the levels of p^{Ser727}STAT3, which colocalizes to the mitochondria (Fig. 5F). Then, we quantified that hypoxia reduced both pSer^{727} and total STAT3 levels in the isolated mitochondrial fraction, which remained low with DISC1 silencing. In contrast, overexpression of DISC1 increased both pSer^{727} and total STAT3 in the mitochondrial fraction (mitoSTAT3) (Fig. 5G). These data suggest that STAT3 localized in the mitochondria contributes to the protective effect of high levels of DISC1 during hypoxia.

Discussion

The unbiased discovery of DISC1 in an *in vitro* CM model of ischemia by RNA sequencing, followed by analyses displaying overrepresentation of risk genes for cardiologic diseases in DISC1 protein interactors, ignited the idea that reduced DISC1 protein levels could be a hitherto unknown regulator of multiple signalling pathways that are important for ischemic cardioprotection. While reperfusion therapies are some of the most successful discoveries in medicine, cardioprotective therapies targeting reperfusion-related injury have not yet been successful and remain one of the top 10 unmet clinical needs in cardiology (Ibanez et al., 2015; Ibanez et al., 2018; Lecour et al., 2014; Parviz et al., 2019). In this study, we show a major negative effect of reduced DISC1 protein levels on myocardial infarct size and CM survival due to disruption of multiple signaling pathways important for cardioprotection during ischemia. In contrast, increasing the protein levels of DISC1 provided enhanced cardiomyocyte survival and activation of cardioprotective signaling.

At the mechanistic level, our data on increased infarct size and cell death following hypoxic challenges by DISC1 depletion are explained by activation of apoptotic signaling. Our first indication of negative signaling was evidenced by an increased release of CytC in CMs exposed to hypoxic stress and DISC1 knockdown. CytC release from mitochondria is an established mechanism for the activation of

caspase-3, which is the key regulatory event that induces terminal effector events in the apoptotic cascade (Earnshaw et al., 1999; Green, 2000; Nicholson et al., 1995; Salvesen, 2002). Upstream, we found that the increased CytC release could be linked to the direct interaction verified in CMs in our data between DISC1 and GSK3β. Here, we reported that knockdown of DISC1 enhanced the activation of GSK3β, whereas overexpression of DISC1 reduced GSK3β activity. These data are important, as recent studies have demonstrated that GSK3β inhibition contributes to cardiac protection in both preconditioning (Juhaszova et al., 2004) and postconditioning (Gomez et al., 2008; Zhu et al., 2006). This protection due to GSK3β inhibition has been linked to hindering opening of the mPTP (Gomez et al., 2008; Juhaszova et al., 2004; Juhaszova et al., 2009; Yang et al., 2017) and consequently the release of proapoptotic molecules into the cytosol (Honda et al., 2005).

Furthermore, our data clearly indicate that reduced levels of DISC1 interrupt a range of signaling processes necessary for cardioprotection. First, we found that knockdown of DISC1 almost completely removed the cardioprotective RISK pathway, evidenced by inactivation of the pro-survival kinase Akt, a downstream target phosphorylated by phosphoinositide 3-kinase (PI3K) signalling (Datta et al., 1997; Fayard et al., 2005; Juhaszova et al., 2004; Kunuthur et al., 2012; Li et al., 2011; Matsui et al., 2001). We also found evidence that knockdown of DISC1 inactivates mTORC2 activity, which has been shown to be necessary for full activation of Akt and cardioprotection (Yano et al., 2014). DISC1 knockdown also hinders the activation of CREB, which has previously been shown to enhance cardioprotection against ischemia (Marais et al., 2008), and to facilitate the protection of neural cells against cerebral ischemia reperfusion injury (Teng et al., 2019). The present data further show that knockdown of DISC1 significantly influences the translocation of STAT3 to the mitochondria. Here, we show that knockdown of DISC1 almost completely removes the phosphorylation of STAT3 at Ser^{727} in the whole lysate as well as in the mitochondria. The loss of mito-STAT3 under hypoxia and DISC1 knockdown was confirmed in the mitochondrial fraction. In contrast, overexpression of DISC1 confirmed increases in both phosphorylated Ser^{727} STAT3 and total mito-STAT3. These data are interesting since the role of active mitoSTAT3 could explain several lines of cardioprotective actions. mitoSTAT3 interacts with and

enhances the activities of complex I and complex II of the ETC and thus facilitates ATP production as well as reduces the production of reactive oxygen species (Wegrzyn et al., 2009). However, in this acute setting, the perhaps most important mechanism for cardioprotection is the direct interaction between mitoSTAT3 and cyclophilin D, the mediator of mPTP opening. Here, the presence of mitoSTAT3 hinders the opening of the mPTP to release Ca^{2+} and CytC, which consequently leads to cell death (Wegrzyn et al., 2009) Accordingly, the loss of mitoSTAT3 during hypoxia and knockdown of DISC1 could explain the increased cell death, whereas increased mitoSTAT3 as a consequence of overexpression of DISC1 could serve as a central mechanism to explain enhanced CM survival during hypoxia. However, the protective role of DISC1 by STAT3 did not act via the SAFE pathways, which refer to the activation of Janus kinase (JAK) and upstream activation of STAT3. Classical canonical activation of STAT3 occurs through receptor activation of the glycoprotein-130-Janus kinase (gp-130-JAK) axis by neuregulin-1 (NRG-1) (in addition to interleukin-6 and tumor necrosis factor α (TNFα),(Wadugu and Kuhn, 2012) leading to JAK phosphorylation of STAT3 at Tyr^{705}. Earlier data showed that in CMs, NRG-1 activation reduced apoptosis after hypoxia-reoxygenation and that intravenous NRG-1 administration reduced MI size following ischemia/reperfusion (Fang et al., 2017). Given that more recent data from neuronal cells show that NRG1-ErbB signaling functions through DISC1 (Unda et al., 2016), we were surprised that we did not find any effect of DISC1 knockdown in this signaling pathway. However, here, we show that DISC1 likely activates STAT3 indirectly via the mTOR and ERK1/2 pathways, which earlier studies have presented as an alternative route of activation by phosphorylation of STAT3 at $pSer^{727}$ (Pipicz et al., 2018; Yokogami et al., 2000).

Altogether, the present study shows that DISC1 is a master regulator in the heart that orchestrates intracellular processes that protect against ischemic heart disease. The findings in the present study could thus have implications for understanding scenarios where functional DISC1 protein expression is compromised during cardiac ischemia, such as in individuals with DISC1 genetic defects. It may also help to elucidate the long-known but unexplained finding that IHD is a major cause of mortality in

patients with severe mental illness (Nielsen et al., 2015; Pillinger et al., 2019; Sun et al., 2019). It is furthermore important to highlight not only the deleterious effects of compromised and reduced DISC1 protein levels, but also the significant effect overexpression of DISC1 has on activating intracellular pro survival signalling and reduced hypoxia induced cell death. This observation may lay the fundament for further progress towards new understanding of how to treat hearts undergoing ischemia. We postulate that a focus on DISC1 in IHD will open avenues for future research and novel diagnostics, which could pave the way for novel targeted treatment strategies.

Materials and methods:

RNA sequencing data - Library construction and sequencing

Total RNA was extracted using a RNeasy Mini Kit from Qiagen (Qiagen Norge, Oslo, Norway) according to the manufacturer's instructions. RNA concentration was measured using a Qubit® RNA HS Assay Kit on a Qubit® 3.0 Fluorometer (Thermo Fisher Scientific Inc., Waltham, MA, USA). Integrity was assessed using an Agilent RNA 6000 Pico Kit on a 2100 Bioanalyzer instrument (Agilent Technologies, Santa Clara, CA, USA).

RNA sequencing libraries were prepared using a TruSeq Stranded mRNA kit (Illumina, San Diego, CA, USA) according to the manufacturer's instructions. In brief, 300 ng of total RNA was used as the starting material. First, mRNA was purified from the total RNA using poly-T oligo-attached magnetic beads, followed by random fragmentation using divalent cations at 94°C for 4 min. First- and second strand cDNAs were synthesized using random oligonucleotides and SuperScript II, followed by DNA polymerase I and RNase H. Exonuclease/polymerase was used to produce blunted overhangs. Illumina dual index adapter oligonucleotides were ligated to cDNA after 3' end adenylation. DNA fragments were enriched by 15 cycles of PCR. The libraries were purified using AMPure XP (Beckman Coulter, Inc., Indianapolis, IN, USA), quantitated by qPCR using the KAPA Library Quantification Kit (Kapa Biosystems, Inc., Wilmington, MA, USA) and validated using the Agilent High Sensitivity DNA Kit on a Bioanalyzer (Agilent Technologies, Santa Clara, CA, USA). The size range of the DNA fragments was measured to be in the range of app. 200-1000 bp and peaked around 285 bp.

Libraries were normalized and pooled to 2.7 pM and subjected to clustering on two NextSeq 500 high output flow cells (Illumina, San Diego, CA, USA). Finally, single-read sequencing was performed for 75 cycles on a NextSeq 500 instrument (Illumina, Inc. San Diego, CA, USA) according to the manufacturer's instructions. Base calling was performed on a NextSeq 500 instrument by RTA 2.4.6. FASTQ files were generated using bcl2fastq2 Conversion Software v2.20.0.422 (Illumina, Inc. San Diego, CA, USA). FASTQ files were filtered and trimmed (fastp v0.20.0), and transcript counts were generated using quasi alignment (Salmon v1.3.0) to the transcriptome reference sequence (Ensembl, GRCh38 release 103). Transcript sequences were imported into R statistical software and aggregated to gene counts using the tximport (v1.14.0) bioconductor package. Gene counts were normalized and analyzed for differential expression using the DESeq2 bioconductor package. DESeq2 is a specialized software for the analysis of RNA-seq data that builds a generalized linear model under the assumption of negative binomial distributed values and uses the Wald statistic for significance testing.

Regulatory networks in hypoxia-stimulated hiPSC-CM relationships between upregulated miRs and their downregulated mRNA targets

Establishing functional relationships between those differentially expressed RNAs, we generated regulatory networks that depicted negative correlations between overexpressed miRNAs and their putative downregulated mRNA transcripts. Regulatory networks in hypoxia-stimulated hiPSC-CM were displayed by the predicted functional relationships between upregulated miRs and their downregulated mRNA targets. All predictions were made by using the MiRWalk 2.0 algorithm(Dweep and Gretz, 2015). Protein-protein interactions were extracted from the STRING database (von Mering et al., 2005).

Data from cardiac patient biopsies

Biopsies were obtained from patients scheduled for elective coronary artery bypass grafting (CABG) at St. Olavs Hospital, Trondheim, Norway (stored in local biobank: ID275364). The patients were post-MI <15 days prior to CABG surgery (MI, N=5) versus patients with no previously defined MI (control, N=4). Biopsies were taken before aortic cross-clamping from nonfibrotic and viable left ventricle mid-myocardium in the remote noninfarcted area using a BioPince™ needle from Angiotech Pharmaceuticals, Inc. (Vancouver, Canada) and snap-frozen in liquid nitrogen. All perioperative procedures were performed according to standard routines of the department. Approved by the Regional Committee for Medical and Health Research Ethics (REK), Norway (Study Id numbers 285936).

Animal studies

The mouse model was a DISC1 locus impairment (DISC1-Li) mouse model that is based on a C57BL/6 background with a locus deletion that included the *Tsnax*/*Trax* gene located at 5' to the *Disc1* gene. The 40-kb locus deleted covers exons 1, 1b, 2 and 3 and depletes *Tsnax*/*Trax-Disc1* intergenic splicing. miRNA in intron 1, which could alter the functions and levels of DISC1 by targeting at least some DISC1-binding partner genes (such as 14-3-3 and CRMP1/2), was also deleted, as previously described (Niwa et al., 2016). (Approved by the Norwegian Animal Research Authority (NARA), Id:13651). Experiments using post myocardial infarction in rats were performed by permanent occlusion of the left anterior descending (LAD) coronary artery, as previously described (Kemi et al., 2007). Sham surgery was performed without ligation. Following MI, the animals remained in their cages before they were killed after 4 weeks. (NARA, Id: 9768).

Langendorff perfused hearts

Global ischemia was performed *ex vivo* on isolated mouse hearts using Langendorff perfusion. After removal of the heart, the aorta was cannulated, and the heart was perfused with Krebs-Hensleit solution with a stable aortic pressure of 60 mmHg and immersed in a bath. Solutions were bubbled with 95% O_2/5% CO_2 and maintained at 37°C. After 20 mins of perfusion, the hearts were subjected to 30 mins of ischemia by stopping the perfusion flow. Hearts were then reperfused for 1 h 40 m before being taken down and frozen at -20°C overnight. The following day, hearts were cut into 1.5 mm transverse sections using a heart slicing matrix and incubated for 10 minutes in 1% 2,3,5-triphenyltetrazolium chloride (TTC) shaking at 37°C. Slices were placed in PBS between glass slides and scanned at 3200 dpi using a flatbed scanner. The second and third slices closest to the apex were used for analysis. Intensity thresholds were determined by a blinded third party to discriminate between black (background), red (viable tissue) and white (nonviable tissue). The percentage of nonviable tissue in a heart was measured by calculating the percentage of white pixels as a total of all non-background pixels across the two section scans. All image analyses were performed using ImageJ. (NARA id: 13651).

Cell culture and treatments: Human AC-16 cardiomyocyte cells (EMD Millipore/Merck Life Sciences, Catalogue # SCC109, Darmstadt, Germany, RRID:CVCL_4U18) were cultured and subcultured in Dulbecco's modified Eagle's medium (DMEM): Ham's F12 (1:1; v/v) with 2 mM glutamine, 12.5% fetal bovine serum (FBS), and 1% antibiotic/antimycotic mix, in accordance with the standard guidelines, procedures, and protocols established by the commercial vendor. For *gain-of-function* and *loss-of-function* experiments, AC-16 cells were *reverse* transfected with the *DISC1* overexpression vector or the vector encoding *DISC1* shRNA (TRC Lentiviral Human DISC1 shRNA, Dharmacon / Horizon Scientific, Cambridge, UK, Catalogue # RHS4533-EG27185). To overexpress or knock-down *DISC1* expression, AC-16 cells were transfected in suspension *(reverse transfection*) with the respective vectors using Polyfect® (Qiagen Norge, Oslo, Norway, Catalogue # 301107) in accordance with the manufacturer's guidelines and standardized procedures (Freshney, 2016). The plasmid load to be transfected was standardized to 1 µg per 0.6 x 10^6 cells and *scaled-up* or *scaled-down* in accordance with the stipulations of the experimental paradigm (Freshney, 2016). Hypoxia challenge (1% O_2, 5% CO_2, and 94% N_2 for 18 hours) was effectuated by incubating the transfected AC-16 cells with specific *hypoxia medium* (*Table S2*). The hypoxia challenge was induced and maintained for the designated duration using the *New Brunswick™ Galaxy® 48 R CO_2 incubator* (Eppendorf Norge AS, Oslo, Norway).

Immunofluorescence confocal image analyzes

AC16 cells were treated as specified, fixed in 4% paraformaldehyde and permeabilized using cold methanol. Following blocking (1 h in PBS with 3% goat serum), proteins were detected using antibodies specific for TOM20 (Santa Cruz Biotechnology, Ca, USA cat. No. 11802-1-AP), DISC1 (Sigma, cat. No. HPA048911), phospho-STAT3^{Ser727} (Cell Signaling Technology, Danvers, MA, USA, cat. 94994) as indicated and visualized by fluorescently labeled secondary antibodies (Alexa Fluor™ 555 goat anti-rabbit and Alexa Fluor™ 488 goat anti-mouse, Invitrogen, A-21428 and A11001, respectively, Thermo Fischer, MA, USA). DNA was stained using Draq5 (5 µM; Thermo Fischer, cat. 62251). Images were acquired using a Zeiss LSM880 Airyscan confocal microscope equipped with a 63 x 1.4 Oil objective. Images were processed using the Zen 2.6 software. All images were deconvolved with Huygens Professional v21.04 (Scientific Volume Imaging, The Netherlands, http://svi.nl) using the CMLE algorithm, with SNR:20 and 40 iterations. Colocalization was analysed using Huygens Professional v21.04 by calculating Manders coefficients(Manders et al., 1993), where M1 represented the degree of colocalization of pSer^{727}STAT3 with TOM20.

Western Blotting: Protein isolation from whole cell lysates was performed using standard protocols (Dennison, 2013), and the protein concentration was determined with the Bradford protein assay. Briefly, treated AC-16 cells were washed 2x with PBS (phosphate-buffered saline), trypsinized to collect the cells and centrifuged at *5000xg*. The pellet was washed again 2x with PBS and homogenized in M-PER™ (mammalian protein extraction reagent) (Thermo Fisher Scientific, Oslo, Norway, Catalogue # 78501) supplemented with protease and phosphatase inhibitors (Halt™ Protease and Phosphatase Inhibitor Cocktail 100x, Thermo Fisher Scientific, Oslo, Norway, Catalogue # 78446). Mitochondrial and cytosolic fractions from the respective experimental groups were prepared using the mitochondrial fractionation kit "*Cytochrome c Release Apoptosis Assay Kit*" from Sigma Aldrich/Merck Millipore (Merck Life Science, Darmstadt, Germany, Catalogue # QIA87) following the manufacturer's protocol and guidelines. For preparing whole cell homogenates from mouse whole *left ventricle* tissue, 30-40 mg of the mouse whole *left ventricle* tissue was *Dounce-homogenized* (Dennison, 2013; Dounce et al., 1955) in RIPA tissue lysis buffer (Tris 50mM, sodium chloride [Nacl] 150mM, Sodium Deoxycholate 0.5% w/v, sodium dodecyl sulphate [SDS] 0.1% w/v, Nonidet P-40 [NP-40] 1% w/v, pH 7.4) (CSHL, 2017) supplemented with protease and phosphatase inhibitors (Halt™ Protease and Phosphatase Inhibitor Cocktail 100x, Thermo Fisher Scientific, Oslo, Norway, Catalogue # 78446) Protein concentrations were determined by the Bradford protein assay method (Bradford, 1976). Proteins (10-50 µg) were resolved on SDS-PAGE gels followed by transfer to a *polyvinylidene*

difluoride (PVDF) membrane (Immun-Blot™ PVDF Membrane, Bio-Rad Norway AS, Oslo, Norway, Catalogue # 1620177) and overnight incubation with the respective primary antibodies at 4°C following standardized protocols(Kurien and Scofield, 2015). The origin, source, and dilutions of the respective antibodies used in this study are compiled in *Table S2*. β-actin was used as a gel loading control for whole cell lysates and cytosolic fractions, while TOM20 was used as a gel loading control for the mitochondrial fractions. The blots were developed with enhanced chemiluminescence substrate (SuperSignal™ West Pico PLUS Chemiluminescent Substrate, Thermo Fisher Scientific, Oslo, Norway, Catalogue # 34580) and imaged using a LICOR Odyssey Fc imaging system (LI-COR Biotechnology, Cambridge, UK). Quantification of the results was performed by densitometry using ImageJ (ImageJ, United States National Institutes of Health, Bethesda, MD, USA, https://imagej.nih.gov/ij/) (Schneider et al., 2012), and the results were analyzed as total integrated densitometric values.

DISC1 ELISA: The DISC1 protein levels in experimental lysates were measured by using a *sandwich ELISA immunoassay* approach (Crowther, 1995). Briefly, 10 ng of DISC1 *capture* antibody (Table S2) was immobilized in each well of a 96-well microplate. The experimental cell lysates (equivalent to 50 µg of protein content) were incubated with the immobilized DISC1 *capture* antibody overnight at 4°C. The conditioned cell lysate was discarded, and the 96-well microplate wells were washed 3x (15 minutes each) with TBS-T (Tris-buffered saline with 0.1% v/v Tween-20) and incubated with the DISC1 *detection* antibody (Table S2) overnight at 4°C. The 96-well microplate wells were washed 3x (15 minutes each) with TBS-T followed by immunodetection with the HRP (horseradish peroxidase)-conjugated secondary antibody using the HRP-substrate TMB (3,3',5,5'-Tetramethylbenzidine) (Thermo Fisher Scientific, Oslo, Norway, Catalogue # N301) as a chromophore for the colorimetric read-out (λ_{450}). The antibody and signal specificity were established by performing a *peptide blocking assay* in the entire gamut of experimental lysates. The *DISC1 antibody blocking peptide* (Thermo Fisher Scientific, Oslo, Norway, Catalogue # PEP-0539) corresponding to the same specific epitope for the DISC1 *detection* antibody (Thermo Fisher Scientific, Oslo, Norway, Catalogue # PA5-20422) was used for the *peptide blocking assay*. The respective optical density (OD) values from the *peptide blocking assay* were used for *experimental blank correction*. Data are expressed as *experimental blank corrected* OD_{450} (λ_{450}) values from three technical replicates for each of the four biological replicates belonging to each experimental group (n = 4).

Co-immunoprecipitation (Co-IP) analysis: Co-immunoprecipitation (Co-IP) assays from the respective experimental AC-16 cell homogenates were performed to determine the relative abundance of GSK3β

in the DISC1 immunoprecipitates. AC-16 cells (1×10^6) seeded in 100 mm plates, transfected and subjected to the experimental interventions (as enunciated earlier), were homogenized using a *nondenaturing* lysis buffer (20 mM Tris, 137 mM NaCl, 2 mM EDTA, 1% Nonidet P-40, 10% glycerol, pH 7.4) supplemented with protease and phosphatase inhibitors. The experimental cell lysates containing 750 µg of total protein were precleared by incubation with protein A/G-coated agarose beads for 30 minutes at 4˚C to reduce the nonspecific binding of proteins to the beads. An equivalent of 750 µg of the precleared lysate was incubated separately with either 5 µg of DISC1 antibody (Table S3) or 5 µg of the corresponding control rabbit IgG antibody (Table S3) overnight at 4˚C. The respective immunocomplexes were captured and immobilized by the addition of protein A/G agarose beads and incubation overnight at 4˚C. The beads containing the immunocomplexes were washed 3x with nondenaturing lysis buffer followed by centrifugation and discarding of the supernatant. The beads were suspended in *denaturing* RIPA buffer (50 mM Tris, 150 mM NaCl, 0.1% SDS, 0.5% sodium deoxycholate, 1% Triton X, pH 7.4) supplemented with protease and phosphatase inhibitors and centrifuged to pellet the beads. The supernatant containing the immunoprecipitated proteins was subjected to *tandem* ELISA or Western blot analysis with the designated antibodies for GSK3β (*Table S3*).

Quantitative *real-time* RT-PCR analysis: Total RNA was extracted from treated AC-16 cells using the "RNeasy Mini Kit" from Qiagen (Qiagen Norge, Oslo, Norway, Catalogue # 74104) following the manufacturer's instructions and protocols. cDNA was obtained by reverse transcribing 1 µg of extracted total RNA using the "QuantiTect Reverse Transcription Kit" from Qiagen (Qiagen Norge, Oslo, Norway, Catalogue # 205313). cDNA amplification was performed using the "miScript SYBR Green PCR Kit" from Qiagen (Qiagen Norge, Oslo, Norway, Catalogue # 218075) following the manufacturer's instructions and protocols. The primer pair used to amplify the *DISC1 mRNA transcript variant L* (NCBI Reference Sequence: NM_018662.3) was as follows: *forward primer 5'-AGAGAGAGAAGGGCTGGAGG-3'* and *reverse primer 5'-TGGAGCTGTAGGCTCTGGAT-3'.* The expression of specific amplified *DISC1* transcripts was normalized to the expression of *actin beta (ACTB)* (NCBI Reference Sequence: NM_001101.5). The primer pair used to amplify the *ACTB mRNA transcript* was as follows: *forward primer 5'- CTCGCCTTTGCCGATCC-3'* and *reverse primer 5'-TCTCCATGTCGTCCCAGTTG-3'.* The expression of specific amplified *DISC1* transcripts was normalized to the expression of *ACTB* using the *delta delta* C_T method.

Cardiac samples from CABG left ventricle myocardium biopsies were stored at -80 °C in RNAlater. After thawing, the biopsies were washed with RNase-free water and excess water remover by bloting againg paper and transferring to new tubes with 4 ceramic beads and 300 µl of RTL lysis buffer. RNA

extraction was performed using an RNeasy kit for fibrous tissues (Qiazol) according the manufacturer's protocol. cDNA was obtained using **a** Quantitech reverse transcription kit (Qiagen) according to the manufacturer's protocol. Quantification was performed by DISC1 Primer Assays from Qiagen (Qiagen QuantiTect Primer Assay (QT01019060) normalized to B2M as a housekeeping gene. For rat tissue, cDNA was obtained using the QuantiTect Reverse Transcription Kit (Qiagen) following the manufacturer's instructions. qRT-PCRs were performed using a QuantiTect SYBR Green PCR Kit (Qiagen). The primer pair used to amplify DISC1 in rats was as follows: *forward primer 5'- GACAGTGGTTGTCGGCAAGAAT-3'* and *reverse primer 5'-TGCTCCAAGCTACATCAAGGC-3'.* PCR amplification was performed using "*CFX96 Real-Time PCR Detection*" from Bio-Rad (Bio-Rad Norway AS, Oslo, Norway) in all samples.

Lactate Dehydrogenase (LDH) Release Assay: The enzymatic activity of the released LDH in the conditioned media was determined as a surrogate measure of generic cell death in response to hypoxia challenge using the "CytoTox 96® Non-Radioactive Cytotoxicity Assay" from Promega (Promega Biotech AB, Nacka, Sweden, Catalogue # G1780) following the manufacturer's instructions and established protocols (Decker and Lohmann-Matthes, 1988). The enzymatic activity of the released LDH was measured by coupled-enzymatic assay that measures the LDH catalyzed conversion of the tetrazolium salt (iodonitrotetrazolium violet; INT) into the respective red *formazan* product(Decker and Lohmann-Matthes, 1988). The magnitude of the red color engendered by the LDH-mediated reduction of the *INT-tetrazolium* compound into the colored *formazan* compound, which is directly proportional to the abundance of LDH released and therefore commensurate to the extent of cell death, was measured by recording the raw optical density values at λ_{490} (490 nm) using a microplate reader. The raw optical density (OD) values measured at λ_{490} (490 nm) were corrected with the *experimental blank*.

MTS Reduction Assay: Cell viability was determined by a surrogate measure of the bioreduction of the *MTS-tetrazolium* compound (Owen's reagent) into the colored *MTS-formazan* compound (CellTiter 96® AQueous One Solution Cell Proliferation Assay [MTS], Promega Biotech AB, Nacka, Sweden, Catalogue # G3580). The magnitude of the color engendered by the bioreduction of the *MTS-tetrazolium* compound into the colored *MTS-formazan* compound, which is directly proportional to the abundance of viable cells, was measured by recording the raw optical density (OD) values at λ_{490} (490 nm) using a microplate reader. The raw optical density (OD) values measured at λ_{490} (490 nm) were corrected with the *experimental blank*.

BrdU Incorporation Assay: BrdU (5-bromo-2'-deoxyuridine) incorporation in proliferating cells was determined as a surrogate measure of cell proliferation. BrdU incorporation in proliferating cells was measured using the "BrdU Cell Proliferation Assay Kit" from Cell Signaling Technology (Cell Signaling Technology, Danvers, MA, USA, Catalogue # 6813) following the manufacturer's protocol and guidelines. For *BrdU incorporation*, AC-16 cells were terminally subcultured, reverse transfected with the respective vectors, and plated in *white opaque, flat clear bottom* 96-well cell culture microplates at a seeding density of $5x10^3$ cells/plate. The cells were incubated for 24 hours posttransfection to ensure progression into the *exponential phase* of cell proliferation. Subsequently, the cells were subjected to 18 hours of hypoxia challenge (as described earlier) in the presence of *labeling medium* containing 10% *BrdU* substrate. For the *BrdU assay*, cells were fixed *in situ,* and the DNA was denatured, followed by immunodetection of the *incorporated BrdU* using a mouse anti-BrdU monoclonal primary antibody and HRP-conjugated anti-mouse IgG secondary antibody (provided with the kit). The magnitude of BrdU-labeled cells was determined by a *colorimetric read-out approach* using TMB solution (provided with the kit) as the HRP substrate. The commensurate development of the color engendered by the HRP substrate TMB, which is directly proportional to the BrdU incorporated, was measured by recording the raw optical density values at λ_{450} (450 nm) using a microplate reader. The raw optical density (OD) values measured at λ_{450} (450 nm) were corrected with the *experimental blank* and subsequently normalized to the protein content.

Caspase-3 Activity Assay: The enzymatic activity of caspase-3 was measured spectrophotometrically using the specific caspase-3 substrate Ac-DEVD-p-NA (N-acetyl- Ac-Asp-Glu-Val-Asp-p-nitroanilide) (Sigma Aldrich, Oslo, Norway, Catalogue # 235400-5MG). Caspase-3 activity was measured as a surrogate of the abundance of the released chromophore engendered by the proteolysis of Ac-DEVD-p-NA by caspase-3 (Nicholson et al., 1995). Briefly, AC-16 cells terminally subcultured and plated in 100 mm cell culture plates to the desired confluence ($4x10^6$ cells per plate) and subjected to the respective transfection and experimental interventions were trypsinized and pelleted by centrifugation (*1000xg* for 5 minutes). The pelleted cells were resuspended in cell lysis buffer (50 mM HEPES, 5 mM CHAPS, pH 7.4) and incubated on ice for 10 minutes to lyse the cells, followed by centrifugation at 12000xg for 15 minutes to pellet the cell debris. The supernatant containing the *nondenatured* cell lysates (devoid of protease inhibitors) was dedicated as input for caspase-3 activity determination. The protein content of the *nondenatured* cell lysates was adjusted to 4 µg/µL, and the volume was adjusted to 180 µL with the addition of assay buffer (20 mM HEPES, 1.62 mM CHAPS, 10 mM NaCl, 2 mM EDTA, pH 7.4). Two hundred micrograms of equivalent protein content (50 µL of the lysate at 4 µg/µL diluted to 180 µL) per well of a 96-well microplate was used as *input* from each

experimental sample for the caspase-3 activity assay. The *input* from the respective samples was incubated with the caspase-3 substrate Ac-DEVD-p-NA (200 µM, 20 µL of 2 mM in a 200 µL assay volume) for 4 hours at 37°C. Caspase-3 activity assays were also performed in the presence of the caspase-3 inhibitor Ac-DEVD-CHO (Nicholson et al., 1995) (Sigma Aldrich/Merck Millipore/Merck Life Science, Darmstadt, Germany, Catalogue # 235420) to exhibit *assay specificity* and serve as an *experimental blank*. The absorbance at λ_{405} (405 nm) corresponding to the amount of the chromophore engendered as a commensurate measure of caspase-3 activity was determined using a microplate reader. The respective optical density (OD) values from the caspase-3 inhibitor-treated lysates were used for *experimental blank correction*.

***Cytochrome c* Release Assay:** The translocation of *cytochrome c* from the intermitochondrial space into the cytosol was determined by using the mitochondrial fractionation kit "*Cytochrome c Release Apoptosis Assay Kit*" from Sigma Aldrich/Merck Millipore (Merck Life Science, Darmstadt, Germany, Catalogue # QIA87) following the manufacturer's protocol. Briefly, AC-16 cells terminally subcultured and plated in 100 mm cell culture plates to the desired confluence ($4x10^6$ cells/plate) and subjected to the respective transfection and experimental interventions (as enunciated earlier) were trypsinized and pelleted by centrifugation (*1000xg* for 5 minutes). The pelleted cells were resuspended in *cytosolic extraction buffer* (supplied with the kit) and incubated on ice for 10 minutes to lyse the cells, followed by centrifugation at *12000xg* for 30 minutes. The resultant supernatant was collected as the *cytosolic fraction*, while the resultant pellet was resuspended in *mitochondrial extraction buffer* (supplied with the kit) to generate the *mitochondrial fraction*. The respective fractions were processed for western blotting analysis following standardized protocols (Kurien and Scofield, 2015) to determine the abundance of *cytochrome c* in the respective fractions. The abundance of *cytochrome c* in the respective fractions was also measured using a *sandwich ELISA immunoassay* approach (Crowther, 1995). Briefly, 20 ng of the *cytochrome c capture* antibody (Table S3) was immobilized in each well of a 96-well microplate (CSHL, 2014). The respective cytosolic fractions and mitochondrial fractions were incubated with the immobilized *cytochrome c capture* antibody overnight at 4°C. The conditioned cytosolic fractions and mitochondrial fractions were discarded, and the 96-well microplate wells were washed 3x (15 minutes each) with TBS-T and incubated with the *cytochrome c detection* antibody (Table S3) overnight at 4°C. The 96-well microplate wells were washed 3x (15 minutes each) with TBS-T followed by immunodetection with the HRP-conjugated secondary antibody using the HRP-substrate OPD (o-phenylenediamine dihydrochloride) (Thermo Fisher Scientific, Oslo, Norway, Catalogue # 34005) as a chromophore for the colorimetric read-out (λ_{450}). The antibody and signal specificity were established by performing a *peptide blocking assay* in the entire gamut of experimental lysates. The

cytochrome c blocking peptide (Cell Signaling Technology, Danvers, MA, USA, Catalogue # 1033) corresponding to the specific epitope for the *cytochrome c* antibody (Cell Signaling Technology, Danvers, MA, USA, Catalogue # 4280) was used for the *peptide blocking assay*. The respective optical density (OD) values from the *peptide blocking assay* were used for *experimental blank correction*.

GSK3β kinase activity assay: The GSK3β kinase activity in *nondenatured* experimental lysates was measured by using an *indirect ELISA immunoassay* approach (Crowther, 1995; Engvall and Perlmann, 1971; Van Weemen and Schuurs, 1971). The extent of phosphorylation of the serine residue in the synthetic peptide (RRRPASVPPSPSLSRHS*(pS)*HQRR) corresponding to the GSK3β consensus recognition motif in the endogenous substrate, muscle glycogen synthase 1 (where (pS) corresponds to phosphorylated serine), was used as a surrogate measure of GSK3β kinase activity in the experimental lysates. Ninety-six-well microplates were prepared utilizing specific *streptavidin-biotin* chemistry (Dundas et al., 2013) following standard procedures (Crowther, 1995; Engvall and Perlmann, 1971; Engvall and Perlmann, 1972). First, 96-well microplate wells were coated with 20 pmol (1.1 µg) of streptavidin (110 µL of 10 µg/mL streptavidin in 20 mM potassium phosphate, pH 6.5) followed by immobilization of the biotinylated GSK3β substrate (GSM [GSK3 substrate peptide], Sigma Aldrich/Merck Life Science, Oslo, Norway, Catalogue # 12-533). The N-terminus biotinylation of the GSK3β substrate-peptide was performed using the "EZ-Link™ NHS-LC-Biotin" biotinylation kit from Thermo Fisher Scientific (Thermo Fisher Scientific, Oslo, Norway, Catalogue # 21336) following the manufacturer's guidelines and established protocols (Diamandis and Christopoulos, 1991; Sélo et al., 1996). Briefly, 50 ng of the biotinylated GSK3β substrate peptide was immobilized in each well of a streptavidin-coated 96-well microplate. The experimental cell lysates (equivalent to 50 µg of protein content) were incubated with the immobilized biotinylated GSK3β substrate overnight at 4°C, followed by incubation for 24 hours with the specific detection primary antibody (100 ng/well, 50 µL of 2 µg/mL) directed against the phosphorylated serine residue (*Table S3).* The abundance of the phosphorylated serine residue in the biotinylated GSK3β substrate was immunodetected with an AP-conjugated secondary antibody (CSHL, 2014) using the AP substrate PNPP (p-nitrophenyl phosphate, disodium salt) as a chromophore for colorimetric read-out (λ_{405}). GSK3β kinase activity assays were also performed in the presence of the GSK3β kinase inhibitor SB-216763 (Coghlan et al., 2000) (Sigma Aldrich/Merck Millipore/Merck Life Science, Darmstadt, Germany, Catalogue # S3442) to exhibit *assay specificity* and serve as an *experimental blank*. The respective optical density (OD) values from the GSK3β kinase inhibitor-treated lysates were used for *experimental blank correction*.

mTORC1 and mTORC2 kinase activity assay: The kinase activities of mTORC1 and mTORC2 were measured in *nondenatured* cell lysates using a modified *immunometric double-antibody sandwich*

(*double-sandwich*) ELISA approach (Kohl and Ascoli, 2017). The abundance of phosphorylated unphosphorylated p70S6K1 at Thr^{389} and the phosphorylation of unphosphorylated Akt at Ser^{473} were considered surrogate measures of mTORC1 and mTORC2 kinase activity, respectively. For the modified *immunometric double-antibody sandwich* ELISA, 96-well microplates were prepared utilizing specific *streptavidin-biotin* chemistry (Dundas et al., 2013) following standard procedures (Crowther, 1995). First, 96-well microplate wells were coated with 20 pmol (1.1 µg) of streptavidin (110 µL of 10 µg/mL streptavidin in 20 mM potassium phosphate, pH 6.5) followed by immobilization of the biotinylated p70S6K1 *capture* antibody (50 ng/well) or the biotinylated Akt *capture* antibody (50 ng/well) (Dundas et al., 2013). The sources of the p70S6K1 antibody and the Akt antibody are provided in *Table S3*. The biotinylation of the p70S6K1 antibody and the Akt antibody was performed using the "*Biotinylation Kit / Biotin Conjugation Kit (Fast, Type B) - Lightning-Link® (ab201796)*" from Abcam (Abcam, Cambridge, UK, Catalogue # ab201796). Subsequently, the aforementioned unphosphorylated substrates, either 50 ng of unphosphorylated p70S6K1 (Abcam, Cambridge, UK, Catalogue # ab167933) or 50 ng of unphosphorylated Akt (Abcam, Cambridge, UK, Catalogue # ab43619), were *affinity captured* in the respective biotinylated antibody-coated wells. The experimental cell lysates, equivalent to 50 µg of protein content of the cell lysates, were incubated with the *affinity captured* unphosphorylated p70S6K1 substrate or the unphosphorylated Akt substrate overnight at 4^0C. The conditioned cell lysates were discarded, and the 96-well microplate wells were washed 3x (15 minutes each) with TBS-T followed by incubation with the respective primary antibodies specific to p-Thr^{389} p70S6K1 or p-Ser^{473} Akt (*Table S3*) overnight at 4°C. The abundance of p-Thr^{389} p70S6K1 and p-Ser^{473} Akt in the respective wells was immunodetected with AP (alkaline phosphatase)-conjugated secondary antibodies (CSHL, 2014) using the AP substrate PNPP (p-nitrophenyl phosphate, disodium salt) (Thermo Fisher Scientific, Oslo, Norway, Catalogue # 37621) as a chromophore for the colorimetric read-out (λ_{405}). The mTORC1 and mTORC2 activity assays were also performed in the presence of the mTOR kinase inhibitor Torin 2 (Liu et al., 2011) to exhibit *assay specificity* and serve as an *experimental blank*. The respective optical density (OD) values from the mTOR kinase inhibitor-treated lysates were used for *experimental blank correction*.

Acknowledgment

The current project was financed by grants from the Research Council Norway – FRIPRO ID 316002. The RNA library prep, sequencing and bioinformatics analysis were performed in close collaboration with the Genomics Core Facility (GCF), Norwegian University of Science and Technology (NTNU). We especially acknowledge Arnar Flatberg for bioinformatics analyses. GCF is funded by the Faculty of Medicine and Health Sciences at NTNU and Central Norway Regional Health Authority. We

acknowledge Dr. Karin Garten for contribution to the method of determining infarct size in TTC stained cardiac tissue. The work with confocal images presented were performed at the Cellular and Molecular Imaging Core Facility (CMIC), Norwegian University of Science and Technology (NTNU). CMIC is funded by the Faculty of Medicine at NTNU and Central Norway Regional Health Authority.

Author contributions:

Conceptualization: MAH

Methodology: GM, MP, NRS, RER, FJE, KY, KI, CAAC, KP, MAH

Investigation: GM, MP, KH, AW, NRS, RER, FJE, KY, KI, CAAC, KP, GB, AS, MAH

Visualization: MAH, GM, KP, NRS

Supervision: MAH, AS

Writing—original draft: MAH

Writing—review & editing: GM, MP, KH, AW, NRS, RER, FJE, KY, KI, CAAC, KP, GB, AS, MAH

Conflict of Interest:

None

References

Barodia, S.K., S.K. Park, K. Ishizuka, A. Sawa, and A. Kamiya. 2015. Half-life of DISC1 protein and its pathological significance under hypoxia stress. *Neurosci Res* 97:1-6.

Bradford, M.M. 1976. A rapid and sensitive method for the quantitation of microgram quantities of protein utilizing the principle of protein-dye binding. *Anal Biochem* 72:248-254.

Brandon, N.J., and A. Sawa. 2011. Linking neurodevelopmental and synaptic theories of mental illness through DISC1. *Nat Rev Neurosci* 12:707-722.

Coghlan, M.P., A.A. Culbert, D.A.E. Cross, S.L. Corcoran, J.W. Yates, N.J. Pearce, O.L. Rausch, G.J. Murphy, P.S. Carter, L. Roxbee Cox, D. Mills, M.J. Brown, D. Haigh, R.W. Ward, D.G. Smith, K.J. Murray, A.D. Reith, and J.C. Holder. 2000. Selective small molecule inhibitors of glycogen synthase kinase-3 modulate glycogen metabolism and gene transcription. *Chemistry & Biology* 7:793-803.

Cross, T.G., D. Scheel-Toellner, N.V. Henriquez, E. Deacon, M. Salmon, and J.M. Lord. 2000. Serine/threonine protein kinases and apoptosis. *Exp. Cell Res.* 256:34-41.

Crowther, J.R. 1995. ELISA. Theory and practice. *Methods Mol Biol* 42:1-218.

CSHL. 2014. Antibodies: A Laboratory Manual, Second edition. Cold Spring Harbor Laboratory Press,

CSHL. 2017. RIPA Lysis Buffer. *Cold Spring Harbor Protocols* 2017:pdb.rec101428.

Datta, S.R., H. Dudek, X. Tao, S. Masters, H. Fu, Y. Gotoh, and M.E. Greenberg. 1997. Akt phosphorylation of BAD couples survival signals to the cell-intrinsic death machinery. *Cell* 91:231-241.

Decker, T., and M.L. Lohmann-Matthes. 1988. A quick and simple method for the quantitation of lactate dehydrogenase release in measurements of cellular cytotoxicity and tumor necrosis factor (TNF) activity. *J Immunol Methods* 115:61-69.

Dennison, C. 2013. A Guide to Protein Isolation. Springer Netherlands,

Diamandis, E.P., and T.K. Christopoulos. 1991. The biotin-(strept)avidin system: principles and applications in biotechnology. *Clin Chem* 37:625-636.

Dounce , A.L., R.F. Witter , K.J. Monty , S. Pate , and M.A. Cottone 1955. A METHOD FOR ISOLATING INTACT MITOCHONDRIA AND NUCLEI FROM THE SAME HOMOGENATE, AND THE INFLUENCE OF MITOCHONDRIAL DESTRUCTION ON THE PROPERTIES OF CELL NUCLEI. *The Journal of Biophysical and Biochemical Cytology* 1:139-153.

Dundas, C.M., D. Demonte, and S. Park. 2013. Streptavidin-biotin technology: improvements and innovations in chemical and biological applications. *Appl Microbiol Biotechnol* 97:9343-9353.

Dweep, H., and N. Gretz. 2015. miRWalk2.0: a comprehensive atlas of microRNA-target interactions. *Nat Methods* 12:697.

Earnshaw, W.C., L.M. Martins, and S.H. Kaufmann. 1999. Mammalian caspases: structure, activation, substrates, and functions during apoptosis. *Annu Rev Biochem* 68:383-424.

Engvall, E., and P. Perlmann. 1971. Enzyme-linked immunosorbent assay (ELISA). Quantitative assay of immunoglobulin G. *Immunochemistry* 8:871-874.

Engvall, E., and P. Perlmann. 1972. Enzyme-Linked Immunosorbent Assay, Elisa. *III. Quantitation of Specific Antibodies by Enzyme-Labeled Anti-Immunoglobulin in Antigen-Coated Tubes* 109:129-135.

Ertracht, O., A. Malka, S. Atar, and O. Binah. 2014. The mitochondria as a target for cardioprotection in acute myocardial ischemia. *Pharmacol. Ther.* 142:33-40.

Fang, S.J., P.Y. Li, C.M. Wang, Y. Xin, W.W. Lu, X.X. Zhang, S. Zuo, C.S. Ma, C.S. Tang, S.P. Nie, and Y.F. Qi. 2017. Inhibition of endoplasmic reticulum stress by neuregulin-1 protects against myocardial ischemia/reperfusion injury. *Peptides* 88:196-207.

Fayard, E., L.A. Tintignac, A. Baudry, and B.A. Hemmings. 2005. Protein kinase B/Akt at a glance. *J. Cell Sci.* 118:5675-5678.

Freshney, R.I. 2016. Culture of Animal Cells: A Manual of Basic Technique and Specialized Applications, 7th Edition. Wiley-Blackwell,

Gomez, L., M. Paillard, H. Thibault, G. Derumeaux, and M. Ovize. 2008. Inhibition of GSK3beta by postconditioning is required to prevent opening of the mitochondrial permeability transition pore during reperfusion. *Circulation* 117:2761-2768.

Green, D.R. 2000. Apoptotic Pathways: Paper Wraps Stone Blunts Scissors. *Cell* 102:1-4.

Griffiths, E.J., and A.P. Halestrap. 1995. Mitochondrial non-specific pores remain closed during cardiac ischaemia, but open upon reperfusion. *Biochem. J.* 307 (Pt 1):93-98.

Halestrap, A.P., S.J. Clarke, and I. Khaliulin. 2007. The role of mitochondria in protection of the heart by preconditioning. *Biochim. Biophys. Acta* 1767:1007-1031.

Hashimoto, R., T. Numakawa, T. Ohnishi, E. Kumamaru, Y. Yagasaki, T. Ishimoto, T. Mori, K. Nemoto, N. Adachi, A. Izumi, S. Chiba, H. Noguchi, T. Suzuki, N. Iwata, N. Ozaki, T. Taguchi, A. Kamiya, A. Kosuga, M. Tatsumi, K. Kamijima, D.R. Weinberger, A. Sawa, and H. Kunugi. 2006. Impact of the DISC1 Ser704Cys polymorphism on risk for major depression, brain morphology and ERK signaling. *Hum Mol Genet* 15:3024-3033.

Hausenloy, D.J., D. Garcia-Dorado, H.E. Botker, S.M. Davidson, J. Downey, F.B. Engel, R. Jennings, S. Lecour, J. Leor, R. Madonna, M. Ovize, C. Perrino, F. Prunier, R. Schulz, J.P.G. Sluijter, L.W. Van Laake, J. Vinten-Johansen, D.M. Yellon, K. Ytrehus, G. Heusch, and P. Ferdinandy. 2017. Novel targets and future strategies for acute cardioprotection: Position Paper of the European Society of Cardiology Working Group on Cellular Biology of the Heart. *Cardiovasc Res* 113:564-585.

Hausenloy, D.J., and D.M. Yellon. 2003. The mitochondrial permeability transition pore: its fundamental role in mediating cell death during ischaemia and reperfusion. *J. Mol. Cell. Cardiol.* 35:339-341.

Honda, H.M., P. Korge, and J.N. Weiss. 2005. Mitochondria and ischemia/reperfusion injury. *Ann N Y Acad Sci* 1047:248-258.

Ibanez, B., G. Heusch, M. Ovize, and F. Van de Werf. 2015. Evolving therapies for myocardial ischemia/reperfusion injury. *J Am Coll Cardiol* 65:1454-1471.

Ibanez, B., S. James, S. Agewall, M.J. Antunes, C. Bucciarelli-Ducci, H. Bueno, A.L.P. Caforio, F. Crea, J.A. Goudevenos, S. Halvorsen, G. Hindricks, A. Kastrati, M.J. Lenzen, E. Prescott, M. Roffi, M. Valgimigli, C. Varenhorst, P. Vranckx, P. Widimsky, and E.S.C.S.D. Group. 2018. 2017 ESC Guidelines for the management of acute myocardial infarction in patients presenting with ST-segment elevation: The Task Force for the management of acute myocardial infarction in patients presenting with ST-segment elevation of the European Society of Cardiology (ESC). *Eur Heart J* 39:119-177.

Juhaszova, M., D.B. Zorov, S.H. Kim, S. Pepe, Q. Fu, K.W. Fishbein, B.D. Ziman, S. Wang, K. Ytrehus, C.L. Antos, E.N. Olson, and S.J. Sollott. 2004. Glycogen synthase kinase-3beta mediates convergence of protection signaling to inhibit the mitochondrial permeability transition pore. *J Clin Invest* 113:1535-1549.

Juhaszova, M., D.B. Zorov, Y. Yaniv, H.B. Nuss, S. Wang, and S.J. Sollott. 2009. Role of glycogen synthase kinase-3beta in cardioprotection. *Circ Res* 104:1240-1252.

Kemi, O.J., M.A. Hoydal, P.M. Haram, A. Garnier, D. Fortin, R. Ventura-Clapier, and O. Ellingsen. 2007. Exercise training restores aerobic capacity and energy transfer systems in heart failure treated with losartan. *Cardiovasc Res* 76:91-99.

Kohl, T.O., and C.A. Ascoli. 2017. Immunometric Double-Antibody Sandwich Enzyme-Linked Immunosorbent Assay. *Cold Spring Harbor Protocols* 2017:pdb.prot093724.

Korkmaz, S., H. Korkmaz, O. Ozer, and M. Atmaca. 2016. Assessment of left ventricle systolic and diastolic functions in schizophrenia patients. *Psychiatry Res* 240:348-351.

Kunuthur, S.P., M.M. Mocanu, B.A. Hemmings, D.J. Hausenloy, and D.M. Yellon. 2012. The Akt1 isoform is an essential mediator of ischaemic preconditioning. *J. Cell. Mol. Med.* 16:1739-1749.

Kurien, B.T., and R.H. Scofield. 2015. Western Blotting - Methods and Protocols. Humana Press,

Lecour, S., H.E. Botker, G. Condorelli, S.M. Davidson, D. Garcia-Dorado, F.B. Engel, P. Ferdinandy, G. Heusch, R. Madonna, M. Ovize, M. Ruiz-Meana, R. Schulz, J.P. Sluijter, L.W. Van Laake, D.M. Yellon, and D.J. Hausenloy. 2014. ESC working group cellular

biology of the heart: position paper: improving the preclinical assessment of novel cardioprotective therapies. *Cardiovasc Res* 104:399-411.

Li, J., W. Xuan, R. Yan, M.B. Tropak, E. Jean-St-Michel, W. Liang, R. Gladstone, P.H. Backx, R.K. Kharbanda, and A.N. Redington. 2011. Remote preconditioning provides potent cardioprotection via PI3K/Akt activation and is associated with nuclear accumulation of beta-catenin. *Clin. Sci. (Lond.)* 120:451-462.

Liu, J.M., A. Liu, J. Leal, F. McMillan, J. Francis, A. Greiser, O.J. Rider, S. Myerson, S. Neubauer, V.M. Ferreira, and S.K. Piechnik. 2017. Measurement of myocardial native T1 in cardiovascular diseases and norm in 1291 subjects. *J Cardiovasc Magn Reson* 19:74.

Liu, Q., J. Wang, S.A. Kang, C.C. Thoreen, W. Hur, T. Ahmed, D.M. Sabatini, and N.S. Gray. 2011. Discovery of 9-(6-aminopyridin-3-yl)-1-(3-(trifluoromethyl)phenyl)benzo[h][1,6]naphthyridin-2(1H)-one (Torin2) as a potent, selective, and orally available mammalian target of rapamycin (mTOR) inhibitor for treatment of cancer. *J Med Chem* 54:1473-1480.

Manders, E.M.M., F.J. Verbeek, and J.A. Aten. 1993. Measurement of co-localization of objects in dual-colour confocal images. *J Microsc* 169:375-382.

Marais, E., S. Genade, and A. Lochner. 2008. CREB activation and ischaemic preconditioning. *Cardiovasc Drugs Ther* 22:3-17.

Matsui, T., J. Tao, F. del Monte, K.H. Lee, L. Li, M. Picard, T.L. Force, T.F. Franke, R.J. Hajjar, and A. Rosenzweig. 2001. Akt activation preserves cardiac function and prevents injury after transient cardiac ischemia in vivo. *Circulation* 104:330-335.

Millar, J.K., J.C. Wilson-Annan, S. Anderson, S. Christie, M.S. Taylor, C.A. Semple, R.S. Devon, D.M. St Clair, W.J. Muir, D.H. Blackwood, and D.J. Porteous. 2000. Disruption of two novel genes by a translocation co-segregating with schizophrenia. *Hum Mol Genet* 9:1415-1423.

Ming, G.L., and H. Song. 2009. DISC1 partners with GSK3beta in neurogenesis. *Cell* 136:990-992.

Nicholson, D.W., A. Ali, N.A. Thornberry, J.P. Vaillancourt, C.K. Ding, M. Gallant, Y. Gareau, P.R. Griffin, M. Labelle, Y.A. Lazebnik, and et al. 1995. Identification and inhibition of the ICE/CED-3 protease necessary for mammalian apoptosis. *Nature* 376:37-43.

Nielsen, J., J. Juel, K.S. Alzuhairi, R. Friis, C. Graff, J.K. Kanters, and S.E. Jensen. 2015. Unrecognised myocardial infarction in patients with schizophrenia. *Acta Neuropsychiatr* 27:106-112.

Niwa, M., T. Cash-Padgett, K.I. Kubo, A. Saito, K. Ishii, A. Sumitomo, Y. Taniguchi, K. Ishizuka, H. Jaaro-Peled, T. Tomoda, K. Nakajima, A. Sawa, and A. Kamiya. 2016. DISC1 a key molecular lead in psychiatry and neurodevelopment: No-More Disrupted-in-Schizophrenia 1. *Mol Psychiatry* 21:1488-1489.

Ohori, K., T. Miura, M. Tanno, T. Miki, T. Sato, S. Ishikawa, Y. Horio, and K. Shimamoto. 2008. Ser9 phosphorylation of mitochondrial GSK-3beta is a primary mechanism of cardiomyocyte protection by erythropoietin against oxidant-induced apoptosis. *Am J Physiol Heart Circ Physiol* 295:H2079-2086.

Organization, W.H. 2014. Global status report on noncommunicable diseases 2014. *WHO.int*

Ozeki, Y., T. Tomoda, J. Kleiderlein, A. Kamiya, L. Bord, K. Fujii, M. Okawa, N. Yamada, M.E. Hatten, S.H. Snyder, C.A. Ross, and A. Sawa. 2003. Disrupted-in-Schizophrenia-1 (DISC-1): mutant truncation prevents binding to NudE-like (NUDEL) and inhibits neurite outgrowth. *Proc Natl Acad Sci U S A* 100:289-294.

Parviz, Y., M. Waleed, S. Vijayan, D. Adlam, S. Lavi, A. Al Nooryani, J. Iqbal, and G.W. Stone. 2019. Cellular and molecular approaches to enhance myocardial recovery after myocardial infarction. *Cardiovasc Revasc Med* 20:351-364.

Pillinger, T., E.F. Osimo, A. de Marvao, M.A. Berry, T. Whitehurst, B. Statton, M. Quinlan, S. Brugger, A. Vazir, S.A. Cook, D.P. O'Regan, and O.D. Howes. 2019. Cardiac structure and function in patients with schizophrenia taking antipsychotic drugs: an MRI study. *Transl Psychiatry* 9:163.

Pipicz, M., V. Demjan, M. Sarkozy, and T. Csont. 2018. Effects of Cardiovascular Risk Factors on Cardiac STAT3. *Int J Mol Sci* 19:

Ruiz-Meana, M., A. Abellan, E. Miro-Casas, E. Agullo, and D. Garcia-Dorado. 2009. Role of sarcoplasmic reticulum in mitochondrial permeability transition and cardiomyocyte death during reperfusion. *Am J Physiol Heart Circ Physiol* 297:H1281-1289.

Salvesen, G.S. 2002. Caspases: opening the boxes and interpreting the arrows. *Cell Death & Differentiation* 9:3-5.

Schneider, C.A., W.S. Rasband, and K.W. Eliceiri. 2012. NIH Image to ImageJ: 25 years of image analysis. *Nature Methods* 9:671-675.

Sciarretta, S., M. Forte, G. Frati, and J. Sadoshima. 2018. New Insights Into the Role of mTOR Signaling in the Cardiovascular System. *Circ Res* 122:489-505.

Sélo, I., L. Négroni, C. Créminon, J. Grassi, and J.M. Wal. 1996. Preferential labeling of alpha-amino N-terminal groups in peptides by biotin: application to the detection of specific anti-peptide antibodies by enzyme immunoassays. *J Immunol Methods* 199:127-138.

Soares, D.C., B.C. Carlyle, N.J. Bradshaw, and D.J. Porteous. 2011. DISC1: Structure, Function, and Therapeutic Potential for Major Mental Illness. *ACS Chem Neurosci* 2:609-632.

Sun, D., L. Li, X. Zhang, T.G. Blanchard, D.R. Fowler, and L. Li. 2019. Causes of Sudden Unexpected Death in Schizophrenia Patients: A Forensic Autopsy Population Study. *Am J Forensic Med Pathol* 40:312-317.

Teng, L., W. Chen, C. Yin, H. Zhang, and Q. Zhao. 2019. Dexmedetomidine Improves Cerebral Ischemia-Reperfusion Injury in Rats via Extracellular Signal-Regulated Kinase/Cyclic Adenosine Monophosphate Response Element Binding Protein Signaling Pathway. *World Neurosurg* 127:e624-e630.

Unda, B.K., V. Kwan, and K.K. Singh. 2016. Neuregulin-1 Regulates Cortical Inhibitory Neuron Dendrite and Synapse Growth through DISC1. *Neural Plast* 2016:7694385.

Van Weemen, B.K., and A.H. Schuurs. 1971. Immunoassay using antigen-enzyme conjugates. *FEBS Lett* 15:232-236.

von Mering, C., L.J. Jensen, B. Snel, S.D. Hooper, M. Krupp, M. Foglierini, N. Jouffre, M.A. Huynen, and P. Bork. 2005. STRING: known and predicted protein-protein associations, integrated and transferred across organisms. *Nucleic Acids Res* 33:D433-437.

Wadugu, B., and B. Kuhn. 2012. The role of neuregulin/ErbB2/ErbB4 signaling in the heart with special focus on effects on cardiomyocyte proliferation. *Am J Physiol Heart Circ Physiol* 302:H2139-2147.

Wegrzyn, J., R. Potla, Y.J. Chwae, N.B. Sepuri, Q. Zhang, T. Koeck, M. Derecka, K. Szczepanek, M. Szelag, A. Gornicka, A. Moh, S. Moghaddas, Q. Chen, S. Bobbili, J. Cichy, J. Dulak, D.P. Baker, A. Wolfman, D. Stuehr, M.O. Hassan, X.Y. Fu, N. Avadhani, J.I. Drake, P. Fawcett, E.J. Lesnefsky, and A.C. Larner. 2009. Function of mitochondrial Stat3 in cellular respiration. *Science* 323:793-797.

Yang, K., Z. Chen, J. Gao, W. Shi, L. Li, S. Jiang, H. Hu, Z. Liu, D. Xu, and L. Wu. 2017. The Key Roles of GSK-3β in Regulating Mitochondrial Activity. *Cell Physiol Biochem* 44:1445-1459.

Yano, T., M. Ferlito, A. Aponte, A. Kuno, T. Miura, E. Murphy, and C. Steenbergen. 2014. Pivotal role of mTORC2 and involvement of ribosomal protein S6 in cardioprotective signaling. *Circ Res* 114:1268-1280.

Yerabham, A.S., O.H. Weiergraber, N.J. Bradshaw, and C. Korth. 2013. Revisiting disrupted-in-schizophrenia 1 as a scaffold protein. *Biol Chem* 394:1425-1437.

Yokogami, K., S. Wakisaka, J. Avruch, and S.A. Reeves. 2000. Serine phosphorylation and maximal activation of STAT3 during CNTF signaling is mediated by the rapamycin target mTOR. *Curr Biol* 10:47-50.

Zhang, M., J. Zheng, R. Nussinov, and B. Ma. 2017. Release of Cytochrome C from Bax Pores at the Mitochondrial Membrane. *Sci Rep* 7:2635.

Zheng, W., H. Wang, Z. Zeng, J. Lin, P.J. Little, L.K. Srivastava, and R. Quirion. 2012. The possible role of the Akt signaling pathway in schizophrenia. *Brain Res* 1470:145-158.

Zhu, M., J. Feng, E. Lucchinetti, G. Fischer, L. Xu, T. Pedrazzini, M.C. Schaub, and M. Zaugg. 2006. Ischemic postconditioning protects remodeled myocardium via the PI3K-PKB/Akt reperfusion injury salvage kinase pathway. *Cardiovasc Res* 72:152-162.

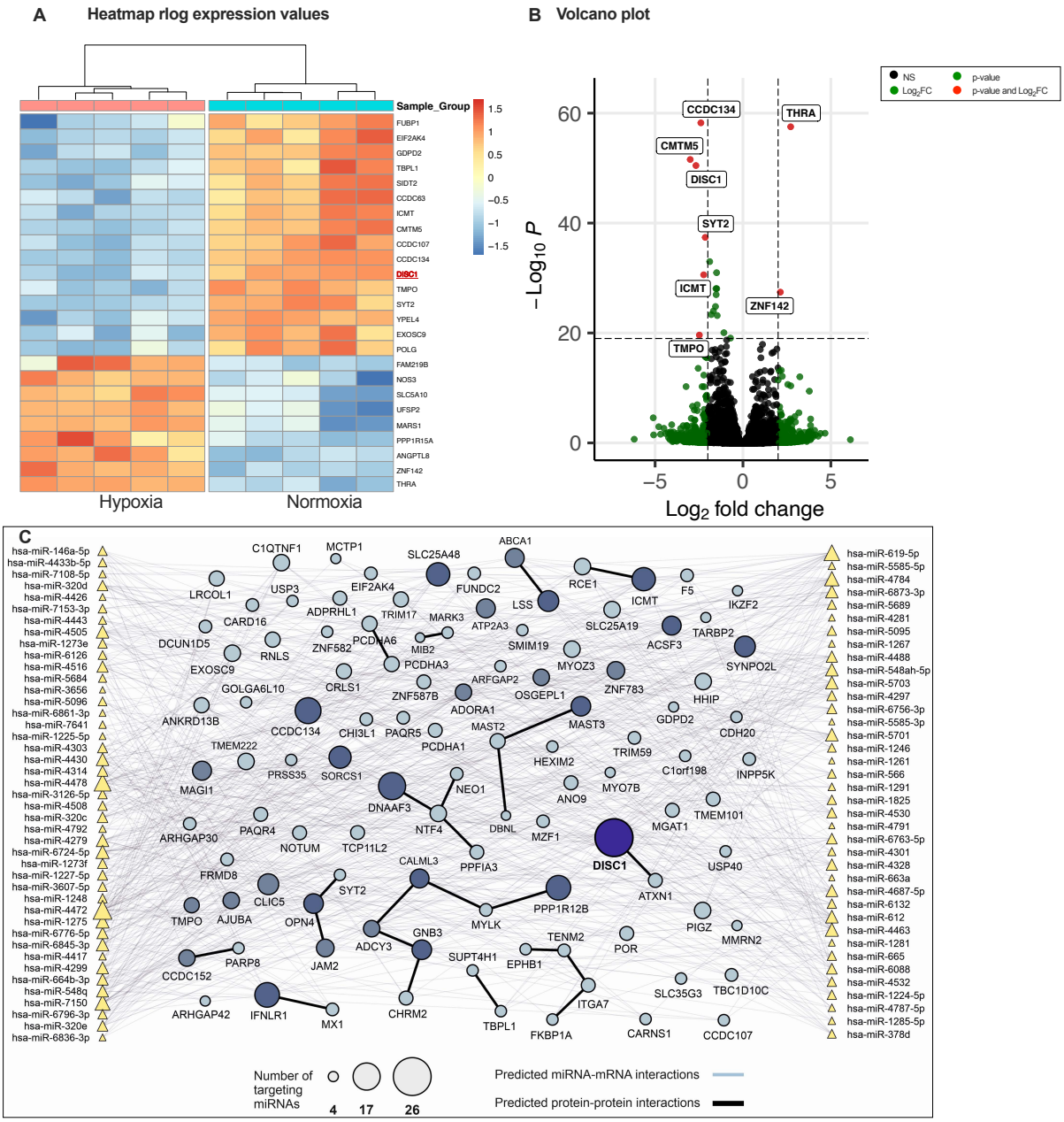

Fig. 1 | Discovering DISC1 by transcriptomics. A, Heatmap of RNA sequencing data of the coding RNA with a cutoff value of $10E^{-10}$ and a Log_2FC cutoff >2. **B**, Volcano plot displaying all regulated coding mRNA transcripts including statistical analyses with cut-off $-Log_{10}$ P value < $10E^{-20}$ and $-Log_2$ fold change value ± 2, MT mRNA are left out for simplicity in A-B. **C**, Regulatory networks in hypoxia-stimulated hIPSC-CM relationships between upregulated microRNAs (miRs) and their downregulated mRNA targets. Upregulated miRNAs are depicted as triangles, whose sizes are related to the number of targets; mRNAs are represented by circles; black lines represent the interaction between proteins encoded by each gene extracted from STRING (combined score >0.8).

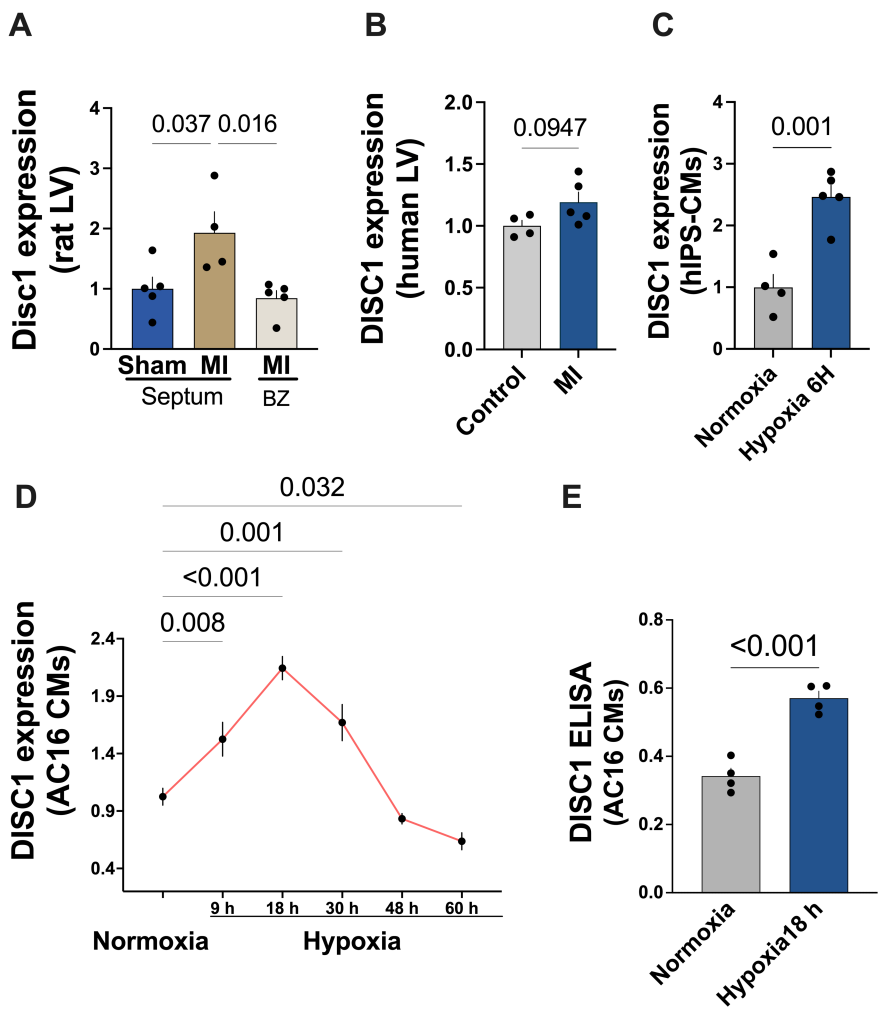

Fig. 2 | Expressional regulation of DISC1 in myocardial infarction and cardiomyocyte hypoxia. A, DISC1 mRNA expression changes in post-myocardial infarction (MI) rat hearts from sham-operated animals and regional areas distant from the MI (sham, N=5; MI septum, N=4: MI border zone (BZ), N=5). **B**, DISC1 mRNA expression in CABG patient biopsies from the left ventricle of post-MI HF patients (N=5) vs. non-MI controls (N=4). **C**, Quantification of DISC1 mRNA transcripts in hiPS-CM following 6 hours of hypoxia (1% O_2). **D**, Timeline of DISC1 mRNA expression in human AC16 CMs following normoxia and hypoxia. **E**, DISC1 total protein expression following 18 hours of hypoxia in AC16 CMs. Data presented as fold change(A-D); E is expressed as absorbances measured at λ_{450} (450 nm), data presented as mean ± s.e.m. P values are indicated. Statistical analyses in A performed by one-way ANOVA and Tukey's post hoc test; B, C and E performed by unpaired t-test; D, performed by one-way ANOVA. All analyses performed using two-tailed analyses.

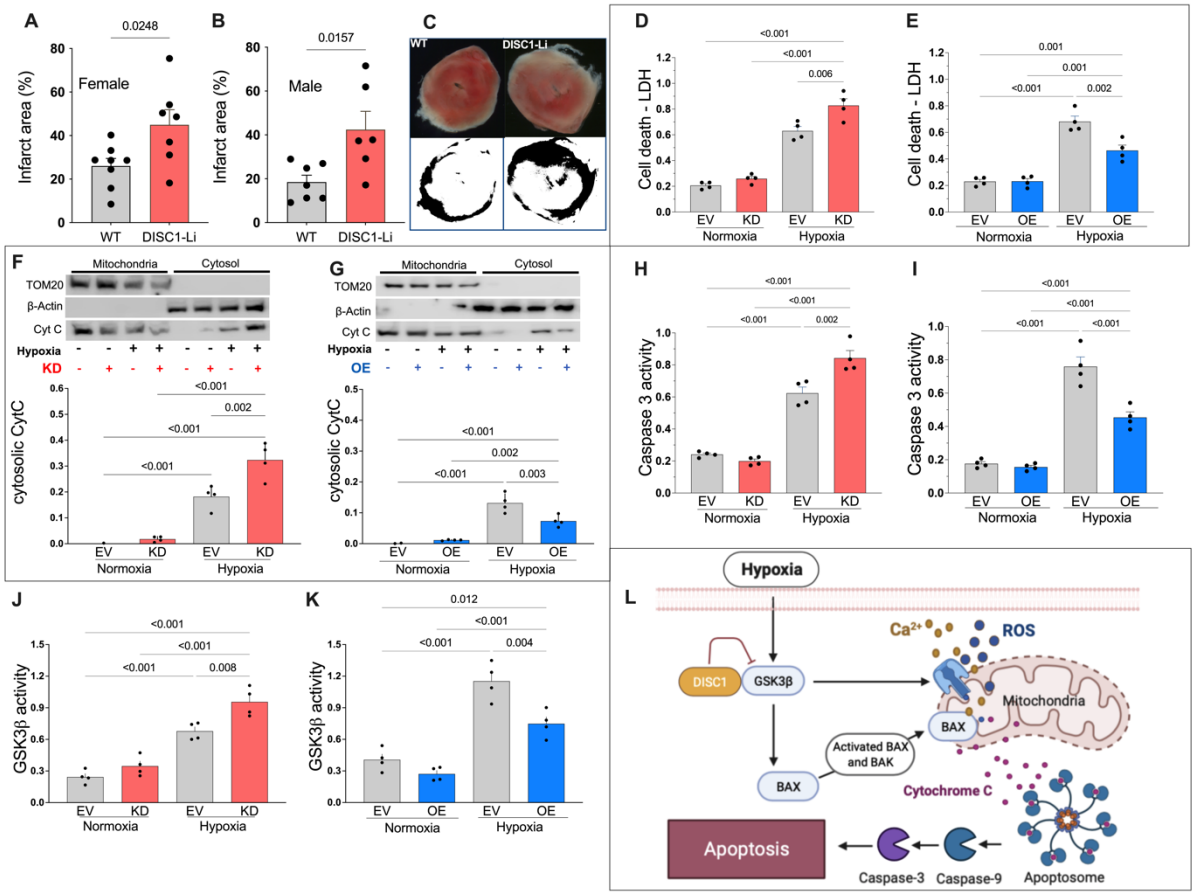

Fig. 3 | Reduced DISC1 protein levels increase myocardial infarction size and promote cell death. **A-B**, Myocardial infarct size in WT and DISC1-Li mice after 30 minutes of global ischemia followed by 1 h 40 m of reperfusion in male mice (WT, n=7/DISC1-Li, n=6) and female mice (WT, n=7/DISC1-Li, n=7). **C**, Exemplary images from WT and DISC-Li Male. The black/white image shows the infarct area in black. **D**, AC16 CMs treated with short hairpin (sh)RNA pLKO.1-DISC1 (knockdown: KD) versus pLKO.1- empty vector (EV) in normoxia and 18 hours of hypoxia (1%). AC16 CMs overexpressing DISC1 (pRK5-DISC1) (overexpression: OE) versus EV. **(E). F**, Quantified levels of cytosolic Cytocrome C (CytC) in normoxic and hypoxic AC16 CMs treated with KD versus EV control. **G**, CytC in AC16 CMs treated with OE of DISC1 versus EV control. In F-G, CytC expression example image of western blot in isolated fractions of mitochondria and (TOM20) cytosol (ß-actin). **H**, Caspase-3 activity after KD of DISC1. **I**, Caspase-3 activity after DISC1 OE versus EV. **J**, Effect of DISC1 KD on GSK3β activity under normoxia and hypoxia. **K**, Effect of DISC1 OE on GSK3ß activity. **L**, Flowchart of the activation of caspase-3 and apoptosis. Data in K-L are expressed as fold change. Data in D-K: N=4 per group, 3 technical replicates. All data are presented as mean ± s.e.m. Statistical analyses were performed by one-way ANOVA with Tukey's post hoc correction for multiple comparisons except A-B, which were analyzed by two-tailed t-test. P values are indicated.

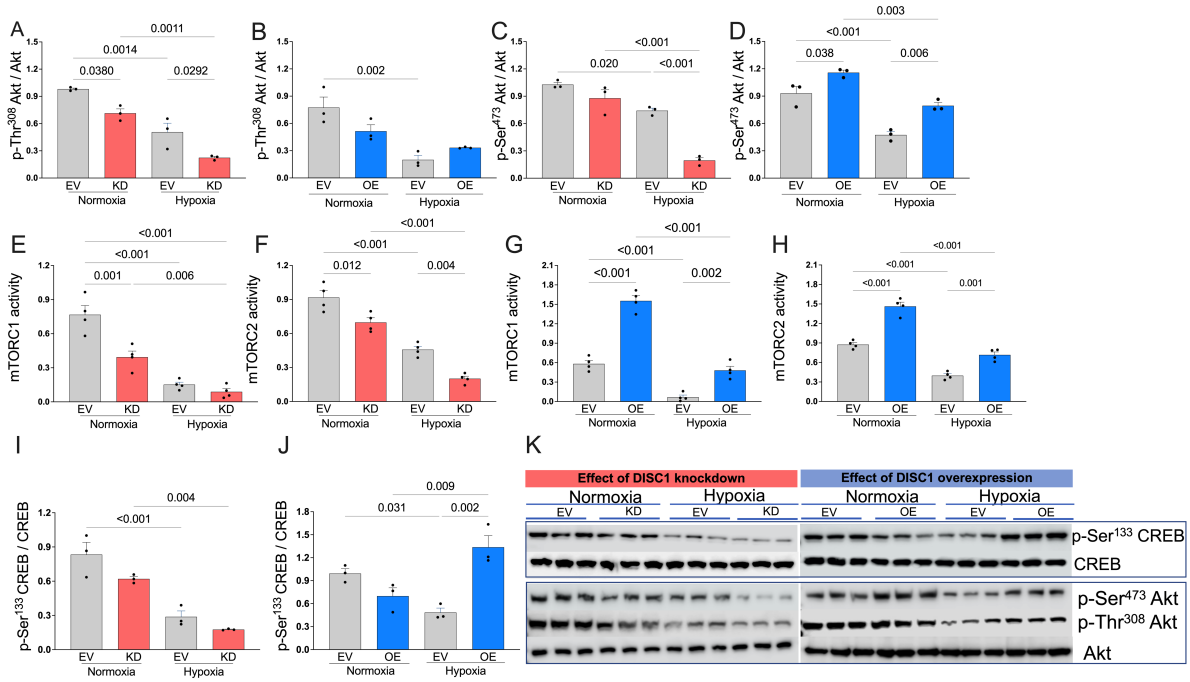

Fig. 4 | Reduced DISC1 expression in cardiomyocytes diminishes prosurvival signaling processes following hypoxic stress. **A-B,** p-Thr308 Akt determined in AC16 CMs treated with either short hairpin (sh)RNA pLKO.1-DISC1 (shRNA-DISC, for knockdown of DISC1: KD of DISC1) versus shRNA pLKO.1- empty vector (EV) or pRK5-DISC1 (for overexpression: OE vs. pRK5. EV) in normoxia and 18 hours of hypoxia (1%). **C-D,** pSer473 Akt protein expression. **E-F**, mTORC1 and mTORC2 activity assay in AC16 CMs with DISC1 KD versus EV in normoxia and hypoxia. **G-H**, mTORC1 and mTORC2 activity assay in DISC1 OE cells vs. EV. **I-J**, Phosphorylated CREB at Ser133. **K**, Exemplary WB for A-D; I-J. Data in A-D are expressed as fold change. All data presented as mean ± s.e.m. Statistical analyses were performed using one-way ANOVA with Tukey's post hoc correction for multiple comparisons. P values are indicated.

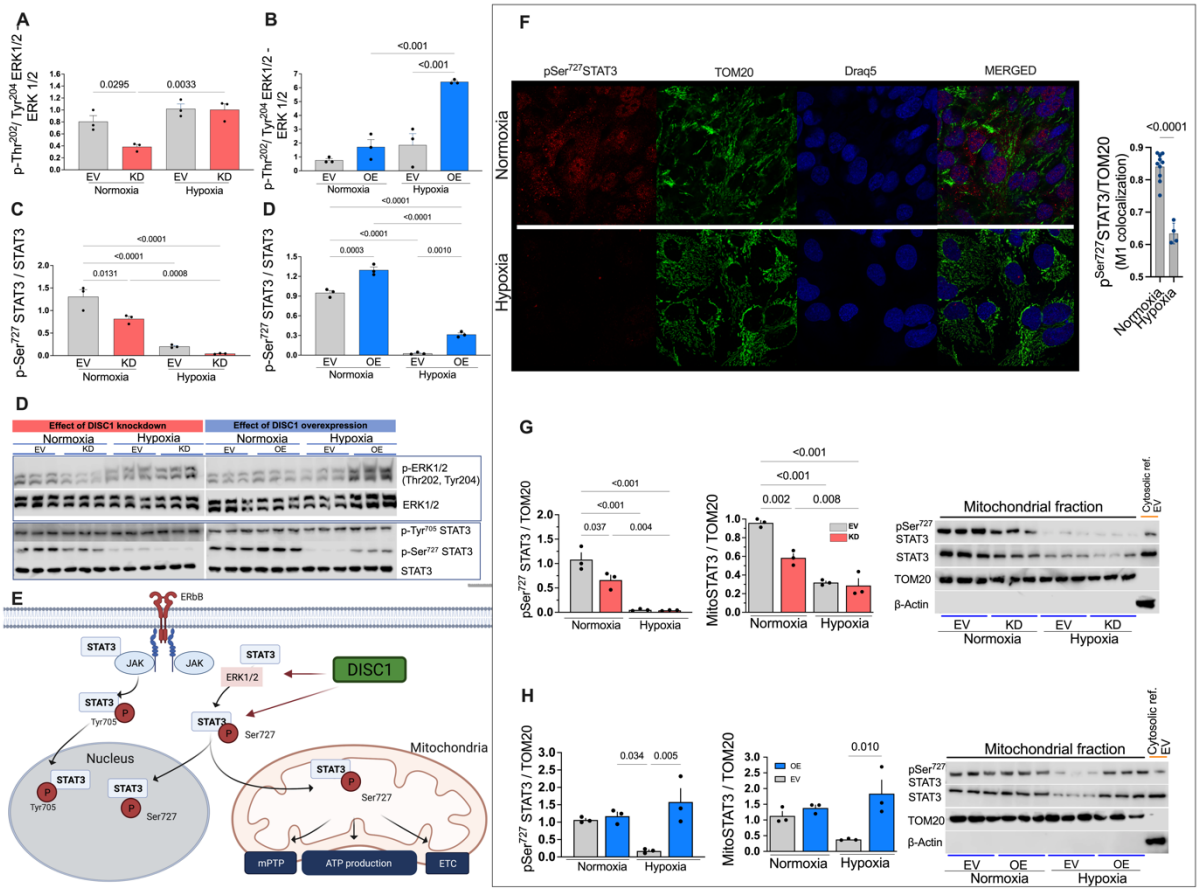

Fig. 5 | Disruption of DISC1 removes cardioprotective STAT3 signaling via ERK1/2. A-B, Phosphorylated ERK1/2 (Thr202, Tyr204) normalized against total ERK1/2 in extracts from AC16 CMs exposed to normoxia or hypoxia and treated with either short hairpin (sh)RNA pLKO.1-DISC1 (shRNA-DISC, for knockdown of DISC1: KD versus shRNA pLKO.1- empty vector (EV) or pRK5-DISC1 (for overexpression: OE vs. pRK5. EV) in normoxia and 18 hours of hypoxia (1%). **C-D**, Analysis performed by western blot for phosphorylated STAT3 at Ser727 (pSer^{727}STAT3). **E**, Diagram of the mechanisms of STAT3 translocation to the nucleus and mitochondria; pSer^{727}STAT3 influences mPTP opening, ATP production and the electron transport chain (ETC). **F**, Exemplary images of normoxic and hypoxic AC16 CMs. Single-channel images with pSER^{727} STAT3, mitochondrial staining using TOM20, nuclear staining using DRAQ5 and merged images. Analyses were performed using Manders M1 colocalization between pSer^{727}STAT3/TOM20 (normoxia, n = 88 cells/10 images; hypoxia, n = 40 cells/4 images). Quantified analyses of the mitochondrial fraction of STAT3 (mitoSTAT3) and pSer^{727}STAT3 in AC16 CMs under normoxia and hypoxic stress stimulation and treated with either EV controls or DISC1 KD for downregulation **(G)** and DISC1 OE versus EV **(H)**. Verification of clean subfractions of mitochondria was controlled by TOM20 and β-actin. Western blot data are presented as fold change. All data presented as mean ± s.e.m. Statistical analyses were performed by one-way ANOVA with Tukey post hoc correction for multiple comparisons, except F where unpaired t-test was used. P values are indicated.